Integrated biological networks associated with platinum-based chemotherapy response in ovarian cancer

Danai Georgia Topouza[a], Jihoon Choi[a], Sean Nesdoly[b], Anastasiya Tarnouskaya[b], Christopher J.B. Nicol[a,c,d], Qing Ling Duan[a,b]

[a]Department of Biomedical and Molecular Sciences, Queen's University, Kingston, Ontario, Canada; [b]School of Computing, Queen's University, Kingston, Ontario, Canada; [c]Department of Pathology and Molecular Medicine, Queen's University, Kingston, Ontario, Canada; [d]Division of Cancer Biology and Genetics, Queen's University Cancer Research Institute, Queen's University, Kingston, Ontario, Canada.

Correspondence: Qing Ling Duan (qingling.duan@queensu.ca)

Abstract

Ovarian cancer is a highly lethal gynecologic cancer, partly due to resistance to platinum-based chemotherapy reported among 20-30% of patients. This study aims to elucidate the biological mechanisms underlying chemotherapy resistance, which remain poorly understood. Using mRNA and microRNA sequencing data from high-grade serous ovarian cancer (HGSOC) patients from The Cancer Genome Atlas, we identified transcripts and networks associated with chemotherapy response. In total, 196 differentially expressed mRNAs were enriched for adaptive immunity and translation, and 21 differentially expressed microRNAs were associated with angiogenesis. Moreover, co-expression network analysis identified two mRNA networks associated with chemotherapy response, which were enriched for ubiquitination and lipid metabolism, as well as three associated microRNA networks enriched for lipoprotein transport and oncogenic pathways. In addition, integrative analyses of these sequence datasets revealed potential regulation of the mRNA networks by the associated microRNAs and single nucleotide polymorphisms. Thus, we report novel transcriptional networks and pathways associated with resistance to platinum-based chemotherapy among HGSOC patients. These results aid our understanding of the effector networks and regulators of chemotherapy response, which will improve drug efficacy and identify novel therapeutic targets for ovarian cancer.

Keywords

Chemotherapy resistance, high-grade serous ovarian cancer (HGSOC), RNA-sequencing, co-expression network analysis, expression quantitative trait loci (eQTL)

Highlights

- mRNA and miRNA transcript networks associated with adjuvant chemotherapy response
- Integrative omics data analysis identified regulatory miRNAs and eQTLs
- Protein ubiquitination and immune activation associated with chemosensitivity
- Increased translation and lipid metabolism may promote chemoresistance

Abbreviations

AOCS: Australian Ovarian Cancer Study
BLCA: Bladder Urothelial Carcinoma
eQTL: Expression Quantitative Trait Locus
ER: Endoplasmic Reticulum
ERAD: Endoplasmic-Reticulum-Associated Protein Degradation
GLM: Generalized Linear Model
HCC: Hepatocellular Carcinoma
HDL: High-Density Lipoprotein
HGSOC: High-Grade Serous Ovarian Cancer
LDL: Low-Density Lipoprotein
miRNA: microRNA
mRNA: Messenger RNA
OC: Ovarian Cancer
OS: Overall Survival
PFI: Platinum-Free Interval
PFS: Progression-Free Survival
PI: Prognostic Index
RNA-Seq: RNA-Sequencing
SNP: Single Nucleotide Polymorphism

TCGA: The Cancer Genome Atlas

TF: Transcription Factor

UPR: Unfolded Protein Response

WGCNA: Weighted Gene Co-Expression Network Analysis

1. Introduction

Ovarian cancer (OC) is a highly lethal gynecologic cancer accounting for 225,000 new cases and 140,000 deaths worldwide each year, the majority of which are high-grade serous ovarian cancer (HGSOC) cases [1]. The first-line standard of care for HGSOC is debulking surgery and platinum-based adjuvant chemotherapy [2]. However, 20-30% of HGSOC patients are resistant to chemotherapy, while the majority of patients who are initially sensitive relapse with chemoresistant disease within three years [2]. Resistant patients have a significantly shorter overall survival (OS) than sensitive patients, and many experience tumor recurrence within six months of completing chemotherapy [3].

Currently, there is no strategy for predicting response to platinum-based chemotherapy, which reflects our limited understanding of the underlying molecular mechanisms of chemotherapy resistance as reviewed elsewhere [4, 5]. Several studies have reported molecular signatures of chemotherapy resistance in OC patients, with little consensus in the results [6]. The majority of these earlier studies used univariate analysis methods such as differential expression analysis, univariate Cox regression, and t-tests that report single gene associations with chemotherapy response in HGSOC [7-10]. The common assumption of these methods is that chemotherapy response is driven by a single gene. However, it is well established that chemotherapy response, like other pharmacogenomics traits, is a complex multifactorial trait modulated by multiple genes contributing to one or more biological pathways [11, 12].

In this study, we apply both univariate and multivariate analysis methods to identify genes and gene networks associated with chemotherapy response in HGSOC. Using mRNA and microRNA (miRNA) sequencing datasets from HGSOC patients of The Cancer Genome Atlas (TCGA) [13], we identify novel transcriptomic differences between patients we define as

sensitive or resistant to platinum-based chemotherapy. Here, we provide the first evidence of novel mRNA and miRNA signalling pathways and networks associated with chemotherapy response in HGSOC patients. We further unveil miRNAs and expression quantitative trait loci (eQTLs) that correlate with the expression of significant transcripts and networks. These findings are validated against two independent cancer cohorts and may provide important therapeutic strategies for regulating platinum-based chemotherapy response in HGSOC patients.

2. Materials and Methods

2.1 Chemotherapy response classification

Sequencing of mRNA and miRNA from the tumors of 191 and 205 HGSOC patients, respectively, prior to chemotherapy were obtained from TCGA [13]. Patients who received platinum-based adjuvant chemotherapy following cytoreductive surgery were selected and separated into sensitive or resistant groups based on their platinum-free interval (PFI) (**Table 1**; see details in **Supplemental Methods**). Sensitive patients remained cancer-free for at least 12 months after completion of chemotherapy, whereas resistant patients experienced cancer recurrence within 6 months of completing chemotherapy. Patients with a recurrence between six months to one year were excluded from analysis in order to enrich for genetic differences between the response groups.

2.2 Processing of RNA sequencing datasets

Raw mRNA-sequence reads were obtained from the TCGA database [13] on August 31st, 2017, as FASTQ files (i.e. level 1 data), filtered for base-quality, aligned, and quantified as described in **Supplemental Methods**. MiRNA-sequencing reads from the same TCGA-HGSOC cohort were obtained as pre-aligned and quantified files (i.e. level 3 data) from the Broad Institute

Genome Data Analysis Center Firehose [14] on September 17th, 2018 (TCGA data version 2016_01_28 for OV). Both mRNA and miRNA expression datasets underwent outlier control, normalization, and non-specific filtering, resulting in 49,116 mRNA transcripts and 4,479 miRNA transcripts for inclusion in further analysis (details in **Supplemental Methods**).

2.3 Differential expression analysis

Differentially expressed mRNA transcripts and miRNA isoforms between sensitive and resistant patients were detected using a negative binomial generalized linear model (GLM) in the DESeq2 R package [15]. This analysis was performed for each individual transcript and controlled for patients' ages at time of diagnosis, as resistant patients were significantly older (**Table 1**). The Benjamini-Hochberg method was applied to correct for multiple testing.

2.4 Weighted co-expression network analysis

The weighted gene co-expression network analysis (WGCNA) R package [16] was used, which applies an unsupervised machine learning approach to identify modules of co-expressed mRNA and miRNA transcripts. Principal component analysis of the expression of all transcripts within each module was calculated, resulting in a value known as the eigengene. Module eigengenes were then used to determine association with chemotherapy response using a GLM, adjusted for patients' age as a covariate (**Supplemental Methods**). Cytoscape was used for visualisation of the gene networks [17].

2.5 Pathway enrichment analysis

Pathway enrichment analysis softwares g:Profiler [18] (rev 1760, database versions Ensembl 93 and Ensembl Genomes 40) and Enrichr [19] were used to determine over-representation of biological pathways from lists of differentially expressed transcripts (mRNA and miRNAs), and

co-expressed networks. In addition, these bioinformatics tools identified enrichment of regulatory motifs, known protein complexes and human phenotype ontologies.

2.6 eQTL analysis

Single nucleotide polymorphisms (SNPs) from TCGA-HGSOC patients were genotyped using the Affymetrix SNP Array 6.0. SNP data was phased and imputed as described by Choi et al. [20]. The imputed data underwent quality control and linkage disequilibrium-based pruning, retaining 1,722,608 common SNPs (minor allele frequency > 0.05) for analysis (**Supplemental Methods, Figure A.3**). This genomics data was integrated with mRNA-seq data of 167 patients and with miRNA-seq data of 178 patients to identify SNPs correlated with transcript expression (i.e. eQTLs) using the MatrixEQTL R package [21]. We tested common SNPs located within 1 Mb of recorded transcripts [22], which included 1,676,365 proximal common SNPs tested for association with mRNAs, and 356,189 proximal common SNPs tested for association with miRNAs (**Supplemental Methods**). Functional annotation of resulting eQTLs was performed using HaploReg v4.1 [23].

2.7 mRNA-microRNA data integration

Potential regulation of mRNA networks by miRNAs was tested using data from 165 patients with both mRNA and miRNA data available. We used the Spearman correlation of module eigengenes from mRNA and miRNA co-expression networks. Results were validated using miRnet [24, 25], a database of experimentally validated mRNA-miRNA interactions, and miRGate [26], a database of predicted mRNA-miRNA interactions based on ribonucleotide motif matching.

2.8 Replication cohort and analysis

Replication of differentially expressed transcripts used the Kaplan-Meier analysis tool KM Plotter [27] to test the association of each transcript with progression-free survival (PFS) or OS in two independent cancer cohorts. First, mRNA data generated from microarrays were analyzed from tumor samples from the Australian Ovarian Cancer Study (AOCS; GSE9891; n=285) [28]. Next, a miRNA dataset from an independent ovarian cancer cohort was not available; we opted to use the bladder urothelial carcinoma cohort (BLCA) (n=409) from TCGA, given that bladder cancer is also typically treated with platinum-based chemotherapy [29]. OS was used as the target phenotype, as PFS was not available for this cohort. Replication of transcript networks used the Prognostic Index (PI) estimation method as described by Aguirre-Gamboa et al. [30] using data from the above cohorts (**Supplemental Methods**).

3. Results

3.1 Differentially expressed mRNAs/miRNAs between sensitive and resistant patients are involved in immune response, translation, and vasculature development

Differential expression analysis identified 196 mRNAs associated with platinum-based chemotherapy response in HGSOC patients (adjusted $p<0.05$) that map to 190 unique genes (**Supplementary Table 2**). A total of 88 transcripts are upregulated in resistant patients, while 108 are downregulated (**Figure 1A**). Pathway enrichment analysis of these associated transcripts using g:Profiler indicated enrichment of 41 annotation terms, including CD22 mediated B-cell receptor regulation, complement activation, and peptide chain elongation (**Table 2, Supplementary Data 1**).

Differential miRNA expression analysis revealed 21 differentially expressed miRNA isoforms (adjusted $p<0.05$), which map to 16 unique miRNAs (**Figure 1B, Supplementary**

Table 3). Pathway enrichment analysis of these miRNA isoforms using g:Profiler revealed 16 pathways and cellular functions such as blood vessel morphogenesis and negative regulation of autophagy (**Table 3, Supplementary Data 1**).

3.2 Two mRNA co-expression networks involved in protein ubiquitination and fatty acid metabolism are associated with chemotherapy response

WGCNA resulted in 58 co-expression modules from the mRNA transcripts (**Supplementary Table 4**), of which two were associated with platinum-based chemotherapy response (**Supplementary Table 5**). First, the *lavenderblush3* module is downregulated or negatively associated with chemotherapy resistance (p-value=0.016; **Figure 2A**). This module contains 39 transcripts, mapping to 31 unique genes (**Figure 2B**). Pathway analysis using g:Profiler indicates enrichment of three biological pathways related to protein ubiquitination, and the transcription factor (TF) GABP-alpha (GA Binding Protein Transcription Factor Subunit Alpha) binding motif (**Table 4**). Second, the *darkolivegreen* module is significantly upregulated in chemoresistant patients (p-value=0.032) (**Figure 2A**) and contains 82 transcripts mapping to 80 unique genes (**Figure 2B**). Enrichr pathway analysis shows that this module is significantly enriched for the protein-containing complex term, as well as for 8 pathways involved in fatty acid metabolism with nominal significance (**Table 4**). Moreover, the *darkolivegreen* module is enriched for 41 TF motifs (**Supplementary Data 1**), with c-Ets-2 (ETS Proto-Oncogene 2) being the most significantly enriched TF motif.

3.3 Three miRNA co-expression networks involved in lipid transport and oncogenic pathways are associated with chemotherapy response

WGCNA analysis of the miRNA dataset constructed 100 co-expression network modules (**Supplementary Table 6**), of which three are associated with chemotherapy response (**Supplementary Table 7**). The *ivory* (p-value=0.0097) and *lightcoral* (p-value=0.042) modules are downregulated or negatively associated with chemotherapy resistance, while the third *plum* network (p-value = 0.045) is positively associated with chemotherapy resistance (**Figure 2C**). The *ivory* network consisted of 25 miRNA isoforms mapping to 11 unique miRNAs, which are enriched for 7 pathways and biological functions, including regulation of lipoprotein transport and negative regulation of cholesterol efflux (**Table 5**). The *lightcoral* module consists of 17 isoforms of miR-187 and the *plum* network consists of 17 isoforms of miR-221 and miR-222 (**Figure 2D**). While no pathway annotations were derived for the *lighcoral* module, the *plum* module is enriched for 18 pathways with a variety of oncogenic functions, such as negative regulation of the TRAIL-activated apoptotic pathway, negative regulation of cell adhesion molecule production, negative regulation of cytokine production involved in inflammatory response, and positive regulation of protein kinase B signaling (**Table 5, Supplementary Data 1**).

3.4 Germline eQTLs may regulate the expression of associated mRNAs, miRNAs, and networks

We identified 268 unique germline cis-eQTLs associated with the expression of mRNAs and miRNAs that are differentially expressed or members of significant co-expression networks. 248 SNPs are associated with the expression of 55 significant mRNAs, and 20 SNPs are associated with the expression of 7 significant miRNAs (**Supplementary Table 8**). Of the 268 eQTLs, 126 are previously known whereas 118 are novel, while 24 are yet not recorded in the HaploReg database. The majority (227) of these eQTLs alter regulatory motifs. Finally, 67 eQTLs are associated with 94 human phenotypes from published Genome-Wide Association Studies

(GWAS). The most common phenotypes associated with these SNPs are related to lipid metabolism, such as high-density lipoprotein (HDL) cholesterol, triglyceride change with statins, and low-density lipoprotein (LDL) cholesterol.

3.5 Network integration reveals novel miRNA-mediated regulation of chemotherapy response mechanisms

Next, we tested for potential interactions between the two significant mRNA modules and the three miRNA modules. The *plum* miRNA network significantly correlates with the *lavenderblush3* mRNA network (Spearman's $\rho = -0.26$, $p < 0.001$), and the *ivory* miRNA network significantly correlates with the *darkolivegreen* mRNA network (Spearman's $\rho = -0.17$, $p = 0.023$) (**Supplementary Table 9**). Annotations using miRnet and miRbase determined that 20 of these mRNA-miRNA interactions are experimentally validated, while 18 others are supported by *in silico* predictions (**Table 6, Figure 3**).

3.6 Replication of study results in two independent cancer cohorts

Kaplan-Meier analysis was used to replicate the association of differentially expressed mRNAs from the TCGA cohort in the second AOCS ovarian cancer cohort. A total of 140 microarray probes in the AOCS dataset (73.68%) matched to differentially expressed genes from TCGA. Of these, 28 (20%) replicated with the same direction of effect (**Supplementary Table 10**). The same analysis was used to test the association of differentially expressed miRNAs from the TCGA-HGSOC cohort in the BLCA cohort from TCGA. Out of the 16 differentially expressed miRNAs, 13 (81.25%) were available in the bladder cancer miRNA-Seq dataset and 7 (53.85%) replicated with the same direction of effect (**Supplementary Table 11**).

Our network analysis results were replicated by applying the PI estimation method [30]. The *lavenderblush3* and *darkolivegreen* mRNA network modules replicated in the AOCS cohort ($p < 0.0001$) (**Figure 4A, B**). In addition, the *ivory* miRNA network module replicated in the TCGA-BLCA cohort ($p = 0.012$), while the *lightcoral* and *plum* modules did not replicate (**Figure 4C-E**). However, differential expression of miR-221 and miR-222, which make up the *plum* network, replicated in this second cohort using Kaplan-Meier analysis ($p = 0.022$ and $p = 0.037$, respectively) (**Figure 4F, G**).

4. Discussion

In this study, we analyzed mRNA and miRNA sequencing data from chemotherapy-naïve tumors of HGSOC patients to identify transcripts and transcript networks associated with chemotherapy response. Our findings implicate novel and known biological pathways that replicated in independent cancer cohorts. In addition, we identified potential interactions among miRNAs and mRNAs, as well as the potential regulation of gene transcripts by SNPs (i.e. expression quantitative trait loci or QTLs). Thus, our results provide an integrative, multi-omics view of gene networks associated with chemotherapy response. This study identifies novel biological targets for further investigation, which will improve our understanding of the mechanisms underlying chemotherapy resistance in HGSOC patients.

We identified one mRNA co-expression network (*lavenderblush3*) significantly upregulated in platinum sensitive patients, which replicated in the AOCS ovarian cancer cohort. The genes within this module are critical for protein processing in the endoplasmic reticulum (ER) and ubiquitin-mediated proteolysis. We also detected a significant downregulation of genes responsible for translation initiation within sensitive patients. These findings suggest that the activation of the unfolded protein response (UPR), a cellular process responsible for resolving

ER stress, may be important in chemotherapy response. The UPR alleviates ER stress through several pathways, including increased endoplasmic-reticulum-associated protein degradation (ERAD) to remove misfolded proteins, and inhibition of translation to reduce protein load in the ER [31]. Our findings indicate that the UPR may be increasingly activated in sensitive patients compared to resistant cases. ER stress, and the ER stress response involving ERAD, promote chemotherapy resistance in ovarian and other cancers [32, 33]. However, the upregulation of ERAD genes such as *VCP* (Valosin Containing Protein), a member of our *lavenderblush3* network, is associated with longer OS and platinum sensitivity in HGSOC patient cohorts [20, 34]. Eighteen of 31 module genes were replicated in an earlier study of the microarray dataset from the same TCGA HGSOC cohort [20].

We identified a second mRNA co-expression network associated with chemotherapy resistance in our HGSOC cohort and replicated in the AOCS cohort. The *darkolivegreen* network included genes associated with fatty acid and cholesterol metabolism (*SREBF1*, *ACAA1*, *ACADV*L), and the Protein Kinase B oncogene (*AKT1*), which promotes de-novo lipid biosynthesis in cancer [35]. Sterol Regulatory Element-Binding Transcription Factor 1 (SREBF1) is a key enzyme for cholesterol and fatty acid synthesis, and an essential gene for ovarian cancer tumor growth whose expression was correlated with the expression of lipogenic genes in ovarian cancer cell lines [36]. *SREBF1* is activated by *AKT1*, promoting fatty acid synthesis [37], which favors cell growth and proliferation in ovarian cancer [38]. Expression of Acyl-CoA Dehydrogenase Very Long Chain (*ACADVL*), which is involved in the β-oxidation of long-chain fatty acids, has been linked to ovarian cancer metastasis and cell survival in suspension [39]. Increased expression of fatty acid synthase, a key enzyme in fatty acid biosynthesis, was an independent prognostic factor for ovarian cancer recurrence [40], while its

inhibition sensitized resistant ovarian cancer cell lines to platinum [41]. Our findings indicate the upregulation of these lipid metabolism genes among chemotherapy resistant patients in the TCGA-HGSOC cohort. Finally, lipid metabolism dysregulation activates the UPR, and the UPR triggers lipid metabolism-based adaptations in the cell through several pathways, including *SREBF1* regulation [42]. The interaction of these two systems may present a link between our gene co-expression networks and warrants further study.

Moreover, our differential expression analysis identified a downregulation of mRNA transcripts encoding for immunoglobulins, B and T lymphocyte factors, and interferon regulatory factors in chemotherapy-resistant patients. The involvement of the immune response is well-known in OC prognosis. Previous studies confirm that a high tumor immune score is a strong predictor of chemosensitivity [43], and that a pre-existing inflammatory tumor microenvironment is associated with increased PFS in HGSOC [44]. There are potential links between this differential immune response activation and our UPR and lipid metabolism-related gene co-expression networks. ER stress can induce pro-inflammatory cytokine production alongside UPR activation in tumor cells [45], but may also be responsible for the disruption of dendritic cell function in the ovarian cancer tumor microenvironment [46]. Finally, increased lipid uptake and fatty acid oxidation inhibit tumor-infiltrating myeloid cell function in various cancers [47-49].

The *ivory* miRNA co-expression network module is enriched for negative regulation of lipoprotein transport, cholesterol efflux and sterol transport. This enrichment is mainly mediated by miR-128-1 and miR-128-2, which play a key role in cholesterol and lipid homeostasis through their suppression of the ABCA1 (ATP Binding Cassette Subfamily A Member 1) cholesterol efflux transporter and the Low-Density Lipoprotein Receptor (LDLR) [50, 51]. MiR-

148a is also a regulator of these key genes [52] which is significantly downregulated in resistant patients. The overexpression of *ABCA1* is associated with reduced survival in OC patients [53], and levels of LDLR are increased in chemoresistant OC cell lines [54]. Finally, overexpression of miR-128 resensitizes resistant OC cells to cisplatin by inhibiting ABCC5 (ATP Binding Cassette Subfamily C Member 5) and BMI-1 (BMI1 ProtoOncogene, Polycomb Ring Finger) [55]. Our results are consistent with the platinum resistance-inhibiting role of miR-128, and its potential activity in cholesterol efflux inhibition alongside miR-148a in this cohort. Elevated cholesterol levels directly contribute to chemotherapy resistance in OC ascites by upregulating drug efflux pump proteins ABCG2 (ATP Binding Cassette Subfamily G Member 2) and ABCB1 (ATP Binding Cassette Subfamily B Member 1) [56], providing a potential mechanism that miR-128 and miR-148a may be intercepting to provide their protective effect in our cohort.

The *plum* miRNA co-expression network consists of multiple isoforms of miR-221 and miR-222, which have been implicated in the development of chemotherapy resistance in OC. MiR-221/miR-222 expression is high in cisplatin-resistant OC cell lines, and its inhibition sensitizes them [57]. Over-expression of miR-221 is associated with reduced disease-free and overall survival, and promotes cell proliferation in OC cell lines through suppression of *APAF1* (Apoptosis Protease Activating Factor 1) [58]. In addition, miR-222 promotes OC cell proliferation by targeting the tumor suppressor $p27^{Kip1}$ (Cyclin-Dependent Kinase Inhibitor 1B) [59]. Our findings are consistent with the increased activity of miR-221 and miR-222 in chemotherapy-resistant HGSOC patient tumors, as previously demonstrated *in vitro*.

Correlation analysis of mRNA-seq and miRNA-seq datasets identified potential interactions of *lavenderblush3* transcripts with miRNAs in the *plum* co-expression module, and between *darkolivegreen* transcripts and miRNAs in the *ivory* co-expression module. The

negative correlation of the *plum* miRNA network with the UPR-associated *lavenderblush3* mRNA network reveals a novel potential mechanism of chemotherapy resistance, as miR-221 and miR-222 may be responsible for the downregulation of this sensitivity-associated gene network in platinum-resistant patients. This finding, combined with the accumulating evidence of miR-221/miR-222 involvement in OC chemoresistance, may point to a promising avenue of therapeutic intervention. However, overexpression of miR-221/miR-222 promotes UPR-induced apoptosis in hepatocellular carcinoma (HCC) cells [60]. While the miR-222-mediated inhibition of $p27^{Kip1}$ promotes cell proliferation in OC, it may also promote apoptosis under ER stress in HCC. ER stress is also responsible for suppressing miR-221/miR-222 in HCC, rendering the cells more resistant to apoptosis. The contribution of this mechanism to chemotherapy response in HGSOC is currently unclear and presents an area for future investigation.

We also identified a negative correlation between the *darkolivegreen* mRNA network and the *ivory* miRNA network. MiRNAs in the *ivory* network, which inhibits lipid transport, may also inhibit lipid metabolism in chemotherapy-sensitive patients through targeting genes in the resistance-associated *darkolivegreen* network. As increased lipid metabolism by cancer cells is a known mechanism of chemotherapy resistance in HGSOC, our finding may present a novel mechanism of chemotherapy sensitivity through miRNA-mediated inhibition of this lipid metabolism-associated network.

Cis-eQTL analysis identified known and novel genomic variants associated with the expression of mRNAs and miRNAs, which are associated with HDL and LDL cholesterol as well as triglyceride levels. High HDL and triglyceride levels correlate with increased cancer stage at diagnosis in epithelial OC patients [61]. In addition, advanced-stage epithelial OC patients with high LDL levels have a significantly shorter PFS compared to patients with normal

LDL levels [62]. Further investigation of these eQTLs is necessary, as they may regulate the expression of transcripts associated with chemotherapy response and may be useful as potential predictors of platinum-based chemotherapy resistance and ovarian cancer prognosis.

Our study improves our understanding of the underlying mechanisms modulating resistance to platinum-based chemotherapy, especially among HGSOC patients, and identifies novel signalling pathways, networks, and regulators. Together, our data may serve as a basis to identify personalized gene signatures to optimize clinical management of patients diagnosed with HGSOC, as well as develop improved therapeutic strategies.

CRediT authorship contribution statement

Danai G. Topouza: Formal analysis, Software, Validation, Writing – Original Draft, Writing – Review & Editing. **Jihoon Choi:** Formal analysis, Software, Writing – Review & Editing. **Sean Nesdoly:** Software, Data Curation. **Anastasiya Tarnouskaya:** Data Curation. **Christopher J.B. Nicol:** Writing – Review & Editing. **Qing Ling Duan:** Conceptualization, Supervision, Methodology, Resources, Funding acquisition, Writing – Review & Editing.

Acknowledgements

Computations in this manuscript were performed on resources and with support provided by the Centre for Advanced Computing (CAC) at Queen's University in Kingston, Ontario. The CAC is funded by the Canada Foundation for Innovation, the Government of Ontario, and Queen's University.

Funding sources

D.G.T. is funded by Queen's University and internal awards in the Department of Biomedical and Molecular Sciences. Q.L.D. receives funding from the Canadian Institutes of Health Research and Queen's University National Scholar Award. The funders did not play any role in the study design, data collection, data analysis, data interpretation, writing of the manuscript or decision to publish results.

Data statement

Transcriptomics, genomics, and clinical data used for the analysis of the TCGA-OV and TCGA-BLCA cohorts can be accessed and downloaded from the Genomic Data Commons (GDC) Data Portal (https://portal.gdc.cancer.gov/). Gene expression and clinical data of the AOCS cohort can be accessed and downloaded from the Gene Expression Omnibus (GEO) database (https://www.ncbi.nlm.nih.gov/geo/query/acc.cgi?acc=GSE9899).

Ethics declarations

Controlled access to datasets from The Cancer Genome Atlas (TCGA) was provided by the National Institute of Health (NIH). The terms of access are outlined in the Data Use Certification Agreement: https://dbgap.ncbi.nlm.nih.gov/aa/wga.cgi?view_pdf&wlid=10654&tlsid=274. Details of the Human subject protection and data access policies implemented by TCGA are as described: https://www.cancer.gov/about-nci/organization/ccg/research/structural-genomics/tcga/history/policies/tcga-human-subjects-data-policies.pdf. Local ethics clearance for human subject research was granted by Queen's University.

Table 1. Characteristics of the HGSOC patient cohorts with mRNA-Seq and miRNA-Seq data from TCGA

	mRNA-Seq cohort				miRNA-Seq cohort			
	Sensitive	**Resistant**	**P value**	**All cases**	**Sensitive**	**Resistant**	**P value**	**All cases**
Age								
Mean (range)	57.15 (30-87)	61.98 (38-87)	**0.0043** [a]	59.22 (30-87)	57.76 (30-87)	61.52 (38-87)	**0.018** [a]	59.26 (30-87)
Grade								
G2	18 (15.93 %)	8 (10.26 %)	0.27 [b]	26 (13.61 %)	23 (18.70 %)	8 (9.76 %)	0.14 [b]	31 (15.12 %)
G3/4	95 (84.07 %)	69 (88.46 %)		164 (85.86 %)	99 (80.49 %)	73 (89.02 %)		172 (83.90 %)
Ungraded	0 (0.00 %)	1 (1.28 %)		1 (0.52 %)	1 (0.81 %)	1 (1.22 %)		2 (0.98 %)
Stage								
II	7 (6.19 %)	2 (2.56 %)	0.48 [b]	9 (4.71 %)	8 (6.50 %)	2 (2.44 %)	0.41 [b]	10 (4.88 %)
III	91 (80.53 %)	67 (85.9 %)		158 (82.72 %)	99 (80.49 %)	67 (81.71 %)		166 (80.98 %)
IV	15 (13.27 %)	9 (11.54 %)		24 (12.57 %)	16 (13.01 %)	13 (15.85 %)		29 (14.15 %)
Cytoreductive surgery outcome								
Optimal (≤ 10mm)	73 (64.60 %)	54 (69.23 %)	0.23 [c]	127 (66.49 %)	77 (62.60 %)	56 (68.29 %)	0.21 [c]	133 (64.88 %)
Suboptimal (> 10mm)	26 (23.01 %)	20 (25.64 %)		46 (24.08 %)	29 (23.58 %)	21 (25.61 %)		50 (24.39 %)
Unknown	14 (12.39 %)	4 (5.13 %)		18 (9.42 %)	17 (13.82 %)	5 (6.10 %)		22 (10.73 %)
Overall survival								
Number of mortality events	48 (42.48 %)	60 (76.92 %)	**2.35E-06** [c]	108 (56.54 %)	55 (44.72 %)	66 (80.49 %)	**0.0002** [c]	121 (59.02 %)
Median months (95% CI)	52.04 (50.07-54.01)	28.2 (26.22-30.18)	**6.97E-10** [a]	39.87 (37.90-41.85)	51.91 (49.94-53.88)	28.2 (26.23-30.18)	**1.13E-10** [a]	39.5 (37.53-41.47)
Adjuvant chemotherapy regimen								
Platinum agent only	4 (3.54 %)	3 (3.85 %)	1 [b]	7 (3.66 %)	4 (3.25 %)	4 (4.88 %)	0.71 [b]	8 (3.90 %)
Platinum/Taxane combination	109 (96.46 %)	75 (96.15 %)		184 (96.34 %)	119 (96.75 %)	78 (95.12 %)		197 (96.10 %)

Primary tumor mRNA subtype								
Differentiated	37 (32.74 %)	22 (28.21 %)	0.49 [b]	59 (30.89 %)	42 (34.15 %)	24 (29.27 %)	0.68 [c]	66 (32.20 %)
Immunoreactive	23 (20.35 %)	10 (12.82 %)		33 (17.28 %)	24 (19.51 %)	13 (15.85 %)		37 (18.05 %)
Mesenchymal	22 (19.47 %)	18 (23.08 %)		40 (20.94 %)	24 (19.51 %)	18 (21.95 %)		42 (20.49 %)
Proliferative	30 (26.55 %)	27 (34.62 %)		57 (29.84 %)	33 (26.83 %)	27 (32.93 %)		60 (29.27 %)
Subtype unknown	1 (0.88 %)	1 (1.28 %)		2 (1.05 %)	0 (0.00 %)	0 (0.00 %)		0 (0.00 %)
Total patients	113	78		191	123	82		205

[a] p-value based on t-test; [b] p-value based on Fisher's Exact test; [c] p-value based on Chi-Squared test

Table 2. Significantly enriched annotation terms for differentially expressed mRNA transcripts

Term name	Adjusted P value	Number of query genes in term
CD22 mediated BCR regulation	4.42E-45	30
Complement activation, classical pathway	3.07E-44	36
Antigen binding	1.74E-42	39
Scavenging of heme from plasma	1.03E-38	28
Immune response-regulating cell surface receptor signaling pathway involved in phagocytosis	3.89E-34	30
Fc-gamma receptor signaling pathway involved in phagocytosis	3.89E-34	30
Serine-type peptidase activity	7.94E-28	28
Cell surface interactions at the vascular wall	2.63E-27	30
Blood microparticle	2.57E-21	25
Leukocyte migration	3.36E-20	33
Immunoglobulin complex	2.24E-09	10
Cell periphery	3.36E-09	80
Plasma membrane	1.37E-08	78
Extracellular exosome	5.22E-07	43
Immunoglobulin receptor binding	5.98E-07	6
Phagocytosis, recognition	1.33E-06	6
External side of plasma membrane	1.48E-06	14
Regulation of B cell activation	8.13E-06	11
Phagocytosis, engulfment	8.91E-06	6
Ribosome	9.44E-05	6
Cytosolic large ribosomal subunit	2.91E-04	6
Ribosome, cytoplasmic	5.57E-04	6
60S ribosomal subunit, cytoplasmic	8.99E-04	5
Formation of a pool of free 40S subunits	9.17E-04	7
Peptide chain elongation	1.39E-03	6
Viral mRNA Translation	1.39E-03	6
Selenocysteine synthesis	1.79E-03	6
Eukaryotic Translation Termination	1.79E-03	6
Abnormal leukocyte morphology	2.02E-03	7
Nonsense Mediated Decay (NMD) independent of the Exon Junction Complex (EJC)	2.02E-03	6
SRP-dependent cotranslational protein targeting to membrane	3.09E-03	6
Nuclear-transcribed mRNA catabolic process, nonsense-mediated decay	4.14E-03	7
Abnormal immunoglobulin level	4.44E-03	5
SRP-dependent cotranslational protein targeting to membrane	5.18E-03	6
Structural constituent of ribosome	6.70E-03	7

Factor: ZNF491; motif: NGKGGKCAGT	1.13E-02	7
Agammaglobulinemia	1.32E-02	2
Verrucae	2.39E-02	2
Cellulitis	4.10E-02	2
TRBP containing complex (DICER, RPL7A, EIF6, MOV10 and subunits of the 60S ribosomal particle)	4.33E-02	4
Nop56p-associated pre-rRNA complex	4.57E-02	5

Table 3. Significantly enriched annotation terms for differentially expressed miRNA isoforms

Term name	Adjusted P value	Number of query miRNAs in term
mRNA binding involved in posttranscriptional gene silencing	4.98E-16	10
Gene silencing by miRNA	7.12E-14	10
MicroRNAs in cancer	1.09E-12	10
Negative regulation of cardiac muscle cell proliferation	5.21E-08	4
Positive regulation of cardiac muscle tissue regeneration	2.10E-07	3
Re-entry into mitotic cell cycle	5.25E-07	3
Negative regulation of cell growth involved in cardiac muscle cell development	8.65E-06	3
Positive regulation of lung blood pressure	2.05E-04	2
Negative regulation of cardiac muscle cell apoptotic process	3.12E-04	3
Regulation of vasculature development	3.32E-03	5
Negative regulation of autophagy	8.70E-03	3
Extracellular space	1.03E-02	9
Positive regulation of connective tissue replacement	2.14E-02	2
Negative regulation of nitric oxide metabolic process	2.45E-02	2
Blood vessel morphogenesis	3.25E-02	5
Positive regulation of protein kinase B signaling	3.97E-02	3

Table 4. Significantly enriched terms in significant mRNA transcript co-expression networks

Network name	Term name	P value	Number of query genes in term
lavenderblush3	Protein modification by small protein conjugation or removal	2.40E-02[a]	9
	Protein modification by small protein conjugation	2.71E-03[a]	9
	Protein ubiquitination	1.60E-03[a]	9
	Factor: GABP-alpha; motif: CTTCCK	6.72E-03[a]	26
darkolivegreen	Protein-containing complex	4.60E-02[a]	37
	Biosynthesis of unsaturated fatty acids	5.20E-03[b]	2
	Fatty acid degradation	1.34E-02[b]	2
	Notch signaling pathway	1.58E-02[b]	2
	Non-alcoholic fatty liver disease (NAFLD)	2.19E-02[b]	3
	Ribosome	2.35E-02[b]	3
	RNA transport	2.85E-02[b]	3
	Synthesis and degradation of ketone bodies	3.93E-02[b]	1
	Peroxisome	4.37E-02[b]	2

[a] Benjamini-Hochberg adjusted p value; [b] non-adjusted p value

Table 5. Significantly enriched terms in significant miRNA isoform co-expression networks

Network name	Term name	Adjusted P value	Number of query miRNAs in term
ivory	mRNA binding involved in posttranscriptional gene silencing	1.16E-09	7
	Gene silencing by miRNA	3.61E-08	7
	Extracellular space	4.24E-05	10
	MicroRNAs in cancer	9.55E-05	5
	Regulation of lipoprotein transport	1.22E-03	2
	Negative regulation of cholesterol efflux	2.69E-02	2
	Negative regulation of lipoprotein particle clearance	4.27E-02	2
plum	Positive regulation of Schwann cell proliferation involved in axon regeneration	2.55E-06	2
	Negative regulation of hematopoietic stem cell proliferation	2.55E-06	2
	Positive regulation of Schwann cell migration	7.66E-06	2
	Negative regulation of TRAIL-activated apoptotic signaling pathway	7.66E-06	2
	Negative regulation of cell adhesion molecule production	1.53E-05	2
	Negative regulation by host of viral genome replication	5.36E-05	2
	Negative regulation of leukocyte adhesion to vascular endothelial cell	1.40E-04	2
	Negative regulation of cytokine production involved in inflammatory response	2.32E-04	2
	Positive regulation of erythrocyte differentiation	1.19E-03	2
	Positive regulation of G1/S transition of mitotic cell cycle	1.61E-03	2
	Positive regulation of vascular smooth muscle cell proliferation	2.53E-03	2
	Positive regulation of epithelial to mesenchymal transition	3.00E-03	2
	Negative regulation of muscle cell differentiation	5.15E-03	2
	Negative regulation of translation, ncRNA-mediated	6.17E-03	2
	Negative regulation of sprouting angiogenesis	8.07E-03	2
	Positive regulation of epithelial cell migration	3.33E-02	2
	Positive regulation of protein kinase B signaling	3.58E-02	2
	mRNA binding involved in posttranscriptional gene silencing	4.25E-02	2

Table 6. Predicted and validated mRNA - miRNA network interactions

Integrated Networks	Gene ID	mRNA ID	miRNA ID	Spearman's ρ	P value	Interaction type	Source
lavenderblush3 - plum	*PSIP1*	ENST00000397519	hsa-mir-222-3p	-0.32	0.000021	Experimental validation	Xue et al. (2013) [1]
	CDC37L1	ENST00000381854	hsa-mir-222-3p	-0.31	0.000042	Computational prediction	Miranda|7mer-m8|889|909|1.11303779449042|;
	CDC37L1	ENST00000381854	hsa-mir-221-3p	-0.27	0.00034	Computational prediction	Miranda|7mer-m8|887|909|1.0718982884376|;
	CDC37L1	ENST00000381854	hsa-mir-221-5p	-0.27	0.00034	Computational prediction	Miranda|8mer|1115|1134|1.3187353247545|;
	CDC37L1	ENST00000381854	hsa-mir-221-5p	-0.27	0.00034	Computational prediction	Miranda|N/A|145|167|1.0718982884376|;
	NFIB	ENST00000380959	hsa-mir-221-3p	-0.27	0.00039	Experimental validation	Grosswendt et al. (2014) [2]
	SMU1	ENST00000397149	hsa-mir-221-5p	-0.26	0.00082	Experimental validation	Kameswaran et al. (2014) [3]
	VCP	ENST00000358901	hsa-mir-222-3p	-0.25	0.00089	Experimental validation	Helwak et al. (2013) [4]
	CAAP1	ENST00000333916	hsa-mir-222-5p	-0.22	0.0041	Computational prediction	Miranda|7mer-m8|1097|1123|1.20902997528032|;
	CAAP1	ENST00000333916	hsa-mir-221-5p	-0.21	0.0076	Computational prediction	Miranda|N/A|694|718|1.14046413185896|;
	TOPORS	ENST00000360538	hsa-mir-221-3p	-0.19	0.014	Experimental validation	Balakrishnan et al. (2014) [5]
	SLC25A51	ENST00000496760	hsa-mir-222-3p	-0.19	0.016	Experimental validation	Helwak et al. (2013) [4]
	PPAPDC2	ENST00000381883	hsa-mir-222-5p	-0.18	0.021	Computational prediction	Microtar|8mer|173|178|-0.863350042828295|;Miranda|7mer-1A|155|179|1.0718982884376|;
	PPAPDC2	ENST00000381883	hsa-mir-222-5p	-0.18	0.021	Computational prediction	Microtar|8mer|1836|1841|-0.87475584746292|;
	VCP	ENST00000358901	hsa-mir-221-3p	-0.17	0.023	Experimental validation	Lipchina et al. (2011) [6]
	VCP	ENST00000358901	hsa-mir-221-5p	-0.17	0.023	Experimental validation	Balakrishnan et al. (2014) [5]
	NFX1	ENST00000379540	hsa-mir-221-5p	-0.17	0.027	Computational prediction	Microtar|7mer-m8|763|768|-0.872619157510717|;Miranda|7mer-m8|748|769|1.09932462580615|;
	PPAPDC2	ENST00000381883	hsa-mir-221-5p	-0.17	0.03	Computational prediction	Miranda|Offset 3-8 6mer|916|937|1.12675096317469|;
	PPAPDC2	ENST00000381883	hsa-mir-221-5p	-0.17	0.03	Computational prediction	Miranda|N/A|132|153|1.05818511975333|;Microtar|7mer-m8|147|152|-0.870278223624131|;
	DNAJA1	ENST00000330899	hsa-mir-221-5p	-0.16	0.035	Experimental validation	Balakrishnan et al. (2014) [5]

	AK3	ENST00000381809	hsa-mir-222-5p	-0.16	0.037	Computational prediction	Miranda|7mer-m8|111|131|1.11303779449042|;
darkolivegreen - ivory	*RPL18*	ENST00000552347	hsa-mir-212-3p	-0.29	0.00017	Experimental Validation	Karginov et al. (2013) [7]
	MRPL55	ENST00000411464	hsa-miR-1306-5p	-0.25	0.001	Computational prediction	Rnahybrid|Offset 3-9 7mer-m8|35|41|-0.874295427824345|;
	FASTK	ENST00000466855	hsa-mir-140-3p	-0.25	0.0013	Experimental Validation	Kishore et al. (2011) [8]
	RPL18	ENST00000552347	hsa-mir-361-3p	-0.24	0.0021	Experimental Validation	Karginov et al. (2013) [7]
	ACBD4	ENST00000321854	hsa-miR-128-2-5p	-0.22	0.0041	Computational prediction	Miranda|7mer-m8|501|523|1.08561145712188|;Rnahybrid|Offset 1-7 7mer-m8|515|522|-0.873597482390991|;
	OAZ1	ENST00000581150	hsa-mir-361-3p	-0.22	0.0047	Experimental Validation	Karginov et al. (2013); Kameswaran et al. (2014) [3, 7]
	ACBD4	ENST00000321854	hsa-miR-128-1-5p	-0.21	0.0059	Computational prediction	Miranda|7mer-m8|500|523|1.0718982884376|;Rnahybrid|Offset 1-7 7mer-m8|515|522|-0.872932832531201|;
	MYL12A	ENST00000578611	hsa-mir-103a-3p	-0.17	0.023	Experimental Validation	Balakrishnan et al. (2014); Karginov et al. (2013) [5, 7]
	MYL12A	ENST00000578611	hsa-mir-107	-0.17	0.023	Experimental Validation	Balakrishnan et al. (2014); Karginov et al. (2013); Nelson et al. (2011) [5, 7, 9]
	HTRA2	ENST00000484352	hsa-mir-1306-5p	-0.17	0.029	Experimental Validation	Karginov et al. (2013) [7]
	ACADVL	ENST00000579425	hsa-mir-103a-3p	-0.17	0.03	Experimental Validation	Balakrishnan et al. (2014) [5]
	ACADVL	ENST00000579425	hsa-mir-107	-0.17	0.03	Experimental Validation	Balakrishnan et al. (2014) [5]
	SOD1	ENST00000470944	hsa-mir-140-3p	-0.16	0.037	Experimental Validation	Xue et al. (2013) [1]
	RHOT2	ENST00000569675	hsa-mir-1306-5p	-0.16	0.044	Experimental Validation	Karginov et al. (2013) [7]
	TSSK6	ENST00000360913	hsa-miR-212-5p	-0.15	0.048	Computational prediction	Microtar|7mer-m8|674|679|-0.874694700443757|;Miranda|N/A|658|680|1.05818511975333|;
	RCC1	ENST00000373832	hsa-miR-1306-3p	-0.15	0.048	Computational prediction	Miranda|7mer-m8|675|693|1.30502215607023|;
	RCC1	ENST00000373832	hsa-miR-1306-5p	-0.15	0.048	Computational prediction	Miranda|7mer-m8|785|805|1.11303779449042|;

[1] Y. Xue, K. Ouyang, J. Huang, Y. Zhou, H. Ouyang, H. Li, G. Wang, Q. Wu, C. Wei, Y. Bi, L. Jiang, Z. Cai, H. Sun, K. Zhang, Y. Zhang, J. Chen, X.D. Fu, Direct conversion of fibroblasts to neurons by reprogramming PTB-regulated microRNA circuits, Cell, 152 (2013) 82-96.
[2] S. Grosswendt, A. Filipchyk, M. Manzano, F. Klironomos, M. Schilling, M. Herzog, E. Gottwein, N. Rajewsky, Unambiguous identification of miRNA:target site interactions by different types of ligation reactions, Mol Cell, 54 (2014) 1042-1054.
[3] V. Kameswaran, N.C. Bramswig, L.B. McKenna, M. Penn, J. Schug, N.J. Hand, Y. Chen, I. Choi, A. Vourekas, K.J. Won, C. Liu, K. Vivek, A. Naji, J.R. Friedman, K.H. Kaestner, Epigenetic regulation of the DLK1-MEG3 microRNA cluster in human type 2 diabetic islets, Cell Metab, 19 (2014) 135-145.

[4] A. Helwak, G. Kudla, T. Dudnakova, D. Tollervey, Mapping the human miRNA interactome by CLASH reveals frequent noncanonical binding, Cell, 153 (2013) 654-665.
[5] I. Balakrishnan, X. Yang, J. Brown, A. Ramakrishnan, B. Torok-Storb, P. Kabos, J.R. Hesselberth, M.M. Pillai, Genome-wide analysis of miRNA-mRNA interactions in marrow stromal cells, Stem Cells, 32 (2014) 662-673.
[6] I. Lipchina, Y. Elkabetz, M. Hafner, R. Sheridan, A. Mihailovic, T. Tuschl, C. Sander, L. Studer, D. Betel, Genome-wide identification of microRNA targets in human ES cells reveals a role for miR-302 in modulating BMP response, Genes Dev, 25 (2011) 2173-2186.
[7] F.V. Karginov, G.J. Hannon, Remodeling of Ago2-mRNA interactions upon cellular stress reflects miRNA complementarity and correlates with altered translation rates, Genes Dev, 27 (2013) 1624-1632.
[8] S. Kishore, L. Jaskiewicz, L. Burger, J. Hausser, M. Khorshid, M. Zavolan, A quantitative analysis of CLIP methods for identifying binding sites of RNA-binding proteins, Nat Methods, 8 (2011) 559-564.
[9] P.T. Nelson, W.X. Wang, G. Mao, B.R. Wilfred, K. Xie, M.H. Jennings, Z. Gao, X. Wang, Specific sequence determinants of miR-15/107 microRNA gene group targets, Nucleic Acids Res, 39 (2011) 8163-8172.

Figure Legends

Figure 1. Differential expression analysis of mRNA and miRNA transcripts. (A) Significant differentially expressed mRNA transcripts (n=196) are shown in red. The Benjamini-Hochberg adjusted significance threshold is indicated by the dashed line. Transcripts with a positive fold change are upregulated in resistant patients, whereas transcripts with a negative fold change are downregulated in resistant patients. (B) Significant differentially expressed miRNA isoforms (n=21) are shown in red. The Benjamini-Hochberg adjusted significance threshold is indicated by the dashed line. Transcripts with a positive fold change are upregulated in resistant patients, whereas transcripts with a negative fold change are downregulated in resistant patients. These figures were generated using the R package ggplot2 (v. 3.3.2) [63].

Figure 2. Weighted transcript co-expression network analysis of mRNA and miRNA transcripts. (A) Heatmap of the correlation between the 58 mRNA co-expression modules with platinum-based chemotherapy resistance, red indicating a positive effect and blue a negative effect. P-values are indicated for each module. Two mRNA co-expression modules are significantly associated with chemotherapy resistance (*lavenderblush3*, *darkolivegreen*). (B) The mRNA modules *lavenderblush3* and *darkolivegreen* are visualized in their respective colors. Each node represents a transcript, and each edge represents a connection or co-expression. The distance between nodes is the connection weight, where more similar transcripts are plotted closer. (C) Heatmap of the correlation between the 100 miRNA modules with platinum-based chemotherapy resistance, red indicating a positive effect and blue a negative effect. P-values are indicated for each module. Three miRNA co-expression modules are significantly associated with chemotherapy resistance (*ivory*, *lightcoral*, and *plum*). (D) The miRNA modules *lightcoral*, *plum*, and *ivory* are visualized in their respective colors. Each node represents one miRNA

isoform, and each edge represents a connection or co-expression. The distance between nodes is the connection weight, where more similar transcripts are plotted closer.

Figure 3. Integration of mRNA - miRNA networks. The mRNA transcripts (oval nodes) from the *lavenderblush3* and *darkolivegreen* modules are arranged based on co-expression similarity (grey edges). Four common miRNA isoforms (rectangular nodes) were validated (orange solid edges) or predicted (orange dashed edges) to regulate the expression of genes in the *lavenderblush3* network module, while 10 miRNA isoforms were validated or predicted to regulate genes in the *darkolivegreen* module. Genes targets of miRNAs indicated by orange border.

Figure 4. Replication analysis of the gene co-expression networks. (A-B) Prognostic Index Kaplan-Meier analysis of patient PFS association with the prognostic index of mRNA networks *lavenderblush3* (A) and *darkolivegreen* (B). (C-E) Prognostic Index Kaplan-Meier analysis of patient OS association with the prognostic index of miRNA networks *ivory* (C), *plum* (D), and *lightcoral* (E). (F-G) Kaplan-Meier analysis of patient OS with the expression of miR-221 (F) and miR-222 (G). Figures 4A-E were generated using the R package survminer (v. 0.4.8) [64]. Figures 4F,G were generated by the KM Plotter tool. PFS, progression-free survival; OS, overall survival.

References

[1] R.J. Kurman, International Agency for Research on Cancer., World Health Organization., WHO classification of tumours of female reproductive organs, 4th ed., International Agency for Research on Cancer, Lyon, 2014.

[2] S. Bouberhan, L. Philp, S. Hill, L.F. Al-Alem, B. Rueda, Exploiting the Prevalence of Homologous Recombination Deficiencies in High-Grade Serous Ovarian Cancer, Cancers (Basel), 12 (2020).

[3] A. Davis, A.V. Tinker, M. Friedlander, "Platinum resistant" ovarian cancer: what is it, who to treat and how to measure benefit?, Gynecol Oncol, 133 (2014) 624-631.

[4] A.E. Freimund, J.A. Beach, E.L. Christie, D.D.L. Bowtell, Mechanisms of Drug Resistance in High-Grade Serous Ovarian Cancer, Hematol Oncol Clin North Am, 32 (2018) 983-996.

[5] M. Binju, M.A. Padilla, T. Singomat, P. Kaur, Y. Suryo Rahmanto, P.A. Cohen, Y. Yu, Mechanisms underlying acquired platinum resistance in high grade serous ovarian cancer - a mini review, Biochim Biophys Acta Gen Subj, 1863 (2019) 371-378.

[6] K.L. Lloyd, I.A. Cree, R.S. Savage, Prediction of resistance to chemotherapy in ovarian cancer: a systematic review, BMC Cancer, 15 (2015) 117.

[7] S. Marchini, R. Fruscio, L. Clivio, L. Beltrame, L. Porcu, I. Fuso Nerini, D. Cavalieri, G. Chiorino, G. Cattoretti, C. Mangioni, R. Milani, V. Torri, C. Romualdi, A. Zambelli, M. Romano, M. Signorelli, S. di Giandomenico, M. D'Incalci, Resistance to platinum-based chemotherapy is associated with epithelial to mesenchymal transition in epithelial ovarian cancer, Eur J Cancer, 49 (2013) 520-530.

[8] M. Koti, R.J. Gooding, P. Nuin, A. Haslehurst, C. Crane, J. Weberpals, T. Childs, P. Bryson, M. Dharsee, K. Evans, H.E. Feilotter, P.C. Park, J.A. Squire, Identification of the IGF1/PI3K/NF kappaB/ERK gene signalling networks associated with chemotherapy resistance and treatment response in high-grade serous epithelial ovarian cancer, BMC Cancer, 13 (2013) 549.

[9] M. Zhang, S.C. Luo, Gene expression profiling of epithelial ovarian cancer reveals key genes and pathways associated with chemotherapy resistance, Genet Mol Res, 15 (2016).

[10] Y. Liu, Z. Zhang, T. Li, X. Li, S. Zhang, Y. Li, W. Zhao, Y. Gu, Z. Guo, L. Qi, A Qualitative Transcriptional Signature for Predicting Recurrence Risk for High-Grade Serous Ovarian Cancer Patients Treated With Platinum-Taxane Adjuvant Chemotherapy, Front Oncol, 9 (2019) 1094.

[11] G. Tapia, I. Diaz-Padilla, Molecular Mechanisms of Platinum Resistance in Ovarian Cancer, Ovarian Cancer - A Clinical and Translational Update, IntechOpen2013.

[12] M. Oti, H.G. Brunner, The modular nature of genetic diseases, Clin Genet, 71 (2007) 1-11.

[13] N. Cancer Genome Atlas Research, Integrated genomic analyses of ovarian carcinoma, Nature, 474 (2011) 609-615.

[14] N. Gehlenborg, M.S. Noble, G. Getz, L. Chin, P.J. Park, Nozzle: a report generation toolkit for data analysis pipelines, Bioinformatics, 29 (2013) 1089-1091.

[15] M.I. Love, W. Huber, S. Anders, Moderated estimation of fold change and dispersion for RNA-seq data with DESeq2, Genome Biol, 15 (2014) 550.

[16] P. Langfelder, S. Horvath, WGCNA: an R package for weighted correlation network analysis, BMC Bioinformatics, 9 (2008) 559.
[17] P. Shannon, A. Markiel, O. Ozier, N.S. Baliga, J.T. Wang, D. Ramage, N. Amin, B. Schwikowski, T. Ideker, Cytoscape: a software environment for integrated models of biomolecular interaction networks, Genome Res, 13 (2003) 2498-2504.
[18] U. Raudvere, L. Kolberg, I. Kuzmin, T. Arak, P. Adler, H. Peterson, J. Vilo, g:Profiler: a web server for functional enrichment analysis and conversions of gene lists (2019 update), Nucleic Acids Res, 47 (2019) W191-W198.
[19] M.V. Kuleshov, M.R. Jones, A.D. Rouillard, N.F. Fernandez, Q. Duan, Z. Wang, S. Koplev, S.L. Jenkins, K.M. Jagodnik, A. Lachmann, M.G. McDermott, C.D. Monteiro, G.W. Gundersen, A. Ma'ayan, Enrichr: a comprehensive gene set enrichment analysis web server 2016 update, Nucleic Acids Res, 44 (2016) W90-97.
[20] J. Choi, D.G. Topouza, A. Tarnouskaya, S. Nesdoly, M. Koti, Q.L. Duan, Gene networks and expression quantitative trait loci associated with adjuvant chemotherapy response in high-grade serous ovarian cancer, BMC Cancer, 20 (2020) 413.
[21] A.A. Shabalin, Matrix eQTL: ultra fast eQTL analysis via large matrix operations, Bioinformatics, 28 (2012) 1353-1358.
[22] B.E. Stranger, S.B. Montgomery, A.S. Dimas, L. Parts, O. Stegle, C.E. Ingle, M. Sekowska, G.D. Smith, D. Evans, M. Gutierrez-Arcelus, A. Price, T. Raj, J. Nisbett, A.C. Nica, C. Beazley, R. Durbin, P. Deloukas, E.T. Dermitzakis, Patterns of cis regulatory variation in diverse human populations, PLoS Genet, 8 (2012) e1002639.
[23] L.D. Ward, M. Kellis, HaploReg v4: systematic mining of putative causal variants, cell types, regulators and target genes for human complex traits and disease, Nucleic Acids Res, 44 (2016) D877-881.
[24] Y. Fan, J. Xia, miRNet-Functional Analysis and Visual Exploration of miRNA-Target Interactions in a Network Context, Methods Mol Biol, 1819 (2018) 215-233.
[25] L. Chang, G. Zhou, O. Soufan, J. Xia, miRNet 2.0: network-based visual analytics for miRNA functional analysis and systems biology, Nucleic Acids Res, 48 (2020) W244-W251.
[26] E. Andres-Leon, G. Gomez-Lopez, D.G. Pisano, Prediction of miRNA-mRNA Interactions Using miRGate, Methods Mol Biol, 1580 (2017) 225-237.
[27] B. Gyorffy, A. Lanczky, Z. Szallasi, Implementing an online tool for genome-wide validation of survival-associated biomarkers in ovarian-cancer using microarray data from 1287 patients, Endocr Relat Cancer, 19 (2012) 197-208.
[28] R.W. Tothill, A.V. Tinker, J. George, R. Brown, S.B. Fox, S. Lade, D.S. Johnson, M.K. Trivett, D. Etemadmoghadam, B. Locandro, N. Traficante, S. Fereday, J.A. Hung, Y.E. Chiew, I. Haviv, G. Australian Ovarian Cancer Study, D. Gertig, A. DeFazio, D.D. Bowtell, Novel molecular subtypes of serous and endometrioid ovarian cancer linked to clinical outcome, Clin Cancer Res, 14 (2008) 5198-5208.
[29] F. Petrelli, A. Coinu, M. Cabiddu, M. Ghilardi, I. Vavassori, S. Barni, Correlation of pathologic complete response with survival after neoadjuvant chemotherapy in bladder cancer treated with cystectomy: a meta-analysis, Eur Urol, 65 (2014) 350-357.
[30] R. Aguirre-Gamboa, H. Gomez-Rueda, E. Martinez-Ledesma, A. Martinez-Torteya, R. Chacolla-Huaringa, A. Rodriguez-Barrientos, J.G. Tamez-Pena, V. Trevino, SurvExpress: an online biomarker validation tool and database for cancer gene expression data using survival analysis, PLoS One, 8 (2013) e74250.

[31] H. Kim, A. Bhattacharya, L. Qi, Endoplasmic reticulum quality control in cancer: Friend or foe, Semin Cancer Biol, 33 (2015) 25-33.
[32] E. Bahar, J.Y. Kim, H. Yoon, Chemotherapy Resistance Explained through Endoplasmic Reticulum Stress-Dependent Signaling, Cancers (Basel), 11 (2019).
[33] J. Tian, R. Liu, Q. Qu, Role of endoplasmic reticulum stress on cisplatin resistance in ovarian carcinoma, Oncol Lett, 13 (2017) 1437-1443.
[34] P. Bastola, L. Neums, F.J. Schoenen, J. Chien, VCP inhibitors induce endoplasmic reticulum stress, cause cell cycle arrest, trigger caspase-mediated cell death and synergistically kill ovarian cancer cells in combination with Salubrinal, Mol Oncol, 10 (2016) 1559-1574.
[35] N. Koundouros, G. Poulogiannis, Reprogramming of fatty acid metabolism in cancer, Br J Cancer, 122 (2020) 4-22.
[36] L.Y. Nie, Q.T. Lu, W.H. Li, N. Yang, S. Dongol, X. Zhang, J. Jiang, Sterol regulatory element-binding protein 1 is required for ovarian tumor growth, Oncol Rep, 30 (2013) 1346-1354.
[37] T. Porstmann, B. Griffiths, Y.L. Chung, O. Delpuech, J.R. Griffiths, J. Downward, A. Schulze, PKB/Akt induces transcription of enzymes involved in cholesterol and fatty acid biosynthesis via activation of SREBP, Oncogene, 24 (2005) 6465-6481.
[38] H.Q. Wang, D.A. Altomare, K.L. Skele, P.I. Poulikakos, F.P. Kuhajda, A. Di Cristofano, J.R. Testa, Positive feedback regulation between AKT activation and fatty acid synthase expression in ovarian carcinoma cells, Oncogene, 24 (2005) 3574-3582.
[39] L.J. Wheeler, Z.L. Watson, L. Qamar, T.M. Yamamoto, B.T. Sawyer, K.D. Sullivan, S. Khanal, M. Joshi, V. Ferchaud-Roucher, H. Smith, L.A. Vanderlinden, S.W. Brubaker, C.M. Caino, H. Kim, J.M. Espinosa, J.K. Richer, B.G. Bitler, Multi-Omic Approaches Identify Metabolic and Autophagy Regulators Important in Ovarian Cancer Dissemination, iScience, 19 (2019) 474-491.
[40] P.L. Alo, P. Visca, M.L. Framarino, C. Botti, S. Monaco, V. Sebastiani, D.E. Serpieri, U. Di Tondo, Immunohistochemical study of fatty acid synthase in ovarian neoplasms, Oncol Rep, 7 (2000) 1383-1388.
[41] E. Papaevangelou, G.S. Almeida, C. Box, N.M. deSouza, Y.L. Chung, The effect of FASN inhibition on the growth and metabolism of a cisplatin-resistant ovarian carcinoma model, Int J Cancer, 143 (2018) 992-1002.
[42] B.A.S. Pinto, L.M. Franca, F.R.M. Laurindo, A.M.A. Paes, Unfolded Protein Response: Cause or Consequence of Lipid and Lipoprotein Metabolism Disturbances?, Adv Exp Med Biol, 1127 (2019) 67-82.
[43] D. Hao, J. Liu, M. Chen, J. Li, L. Wang, X. Li, Q. Zhao, L.J. Di, Immunogenomic Analyses of Advanced Serous Ovarian Cancer Reveal Immune Score is a Strong Prognostic Factor and an Indicator of Chemosensitivity, Clin Cancer Res, 24 (2018) 3560-3571.
[44] M. Koti, A. Siu, I. Clément, M. Bidarimath, G. Turashvili, A. Edwards, K. Rahimi, A.M. Mes-Masson, J.A. Squire, A distinct pre-existing inflammatory tumour microenvironment is associated with chemotherapy resistance in high-grade serous epithelial ovarian cancer, Br J Cancer, 112 (2015) 1215-1222.
[45] N.R. Mahadevan, J. Rodvold, H. Sepulveda, S. Rossi, A.F. Drew, M. Zanetti, Transmission of endoplasmic reticulum stress and pro-inflammation from tumor cells to myeloid cells, Proc Natl Acad Sci U S A, 108 (2011) 6561-6566.
[46] J.R. Cubillos-Ruiz, P.C. Silberman, M.R. Rutkowski, S. Chopra, A. Perales-Puchalt, M. Song, S. Zhang, S.E. Bettigole, D. Gupta, K. Holcomb, L.H. Ellenson, T. Caputo, A.H. Lee, J.R.

Conejo-Garcia, L.H. Glimcher, ER Stress Sensor XBP1 Controls Anti-tumor Immunity by Disrupting Dendritic Cell Homeostasis, Cell, 161 (2015) 1527-1538.
[47] D.L. Herber, W. Cao, Y. Nefedova, S.V. Novitskiy, S. Nagaraj, V.A. Tyurin, A. Corzo, H.I. Cho, E. Celis, B. Lennox, S.C. Knight, T. Padhya, T.V. McCaffrey, J.C. McCaffrey, S. Antonia, M. Fishman, R.L. Ferris, V.E. Kagan, D.I. Gabrilovich, Lipid accumulation and dendritic cell dysfunction in cancer, Nat Med, 16 (2010) 880-886.
[48] F. Hossain, A.A. Al-Khami, D. Wyczechowska, C. Hernandez, L. Zheng, K. Reiss, L.D. Valle, J. Trillo-Tinoco, T. Maj, W. Zou, P.C. Rodriguez, A.C. Ochoa, Inhibition of Fatty Acid Oxidation Modulates Immunosuppressive Functions of Myeloid-Derived Suppressor Cells and Enhances Cancer Therapies, Cancer Immunol Res, 3 (2015) 1236-1247.
[49] R. Ramakrishnan, V.A. Tyurin, F. Veglia, T. Condamine, A. Amoscato, D. Mohammadyani, J.J. Johnson, L.M. Zhang, J. Klein-Seetharaman, E. Celis, V.E. Kagan, D.I. Gabrilovich, Oxidized lipids block antigen cross-presentation by dendritic cells in cancer, J Immunol, 192 (2014) 2920-2931.
[50] A. Wagschal, S.H. Najafi-Shoushtari, L. Wang, L. Goedeke, S. Sinha, A.S. deLemos, J.C. Black, C.M. Ramirez, Y. Li, R. Tewhey, I. Hatoum, N. Shah, Y. Lu, F. Kristo, N. Psychogios, V. Vrbanac, Y.C. Lu, T. Hla, R. de Cabo, J.S. Tsang, E. Schadt, P.C. Sabeti, S. Kathiresan, D.E. Cohen, J. Whetstine, R.T. Chung, C. Fernandez-Hernando, L.M. Kaplan, A. Bernards, R.E. Gerszten, A.M. Naar, Genome-wide identification of microRNAs regulating cholesterol and triglyceride homeostasis, Nat Med, 21 (2015) 1290-1297.
[51] Y.K. Adlakha, S. Khanna, R. Singh, V.P. Singh, A. Agrawal, N. Saini, Pro-apoptotic miRNA-128-2 modulates ABCA1, ABCG1 and RXRalpha expression and cholesterol homeostasis, Cell Death Dis, 4 (2013) e780.
[52] L. Goedeke, N. Rotllan, A. Canfran-Duque, J.F. Aranda, C.M. Ramirez, E. Araldi, C.S. Lin, N.N. Anderson, A. Wagschal, R. de Cabo, J.D. Horton, M.A. Lasuncion, A.M. Naar, Y. Suarez, C. Fernandez-Hernando, MicroRNA-148a regulates LDL receptor and ABCA1 expression to control circulating lipoprotein levels, Nat Med, 21 (2015) 1280-1289.
[53] E.L. Hedditch, B. Gao, A.J. Russell, Y. Lu, C. Emmanuel, J. Beesley, S.E. Johnatty, X. Chen, P. Harnett, J. George, G. Australian Ovarian Cancer Study, R.T. Williams, C. Flemming, D. Lambrechts, E. Despierre, S. Lambrechts, I. Vergote, B. Karlan, J. Lester, S. Orsulic, C. Walsh, P. Fasching, M.W. Beckmann, A.B. Ekici, A. Hein, K. Matsuo, S. Hosono, T. Nakanishi, Y. Yatabe, T. Pejovic, Y. Bean, F. Heitz, P. Harter, A. du Bois, I. Schwaab, E. Hogdall, S.K. Kjaer, A. Jensen, C. Hogdall, L. Lundvall, S.A. Engelholm, B. Brown, J. Flanagan, M.D. Metcalf, N. Siddiqui, T. Sellers, B. Fridley, J. Cunningham, J. Schildkraut, E. Iversen, R.P. Weber, A. Berchuck, E. Goode, D.D. Bowtell, G. Chenevix-Trench, A. deFazio, M.D. Norris, S. MacGregor, M. Haber, M.J. Henderson, ABCA transporter gene expression and poor outcome in epithelial ovarian cancer, J Natl Cancer Inst, 106 (2014).
[54] L. Zheng, L. Li, Y. Lu, F. Jiang, X.A. Yang, SREBP2 contributes to cisplatin resistance in ovarian cancer cells, Exp Biol Med (Maywood), 243 (2018) 655-662.
[55] B. Li, H. Chen, N. Wu, W.J. Zhang, L.X. Shang, Deregulation of miR-128 in ovarian cancer promotes cisplatin resistance, Int J Gynecol Cancer, 24 (2014) 1381-1388.
[56] S. Kim, M. Lee, D.N. Dhanasekaran, Y.S. Song, Activation of LXRa/beta by cholesterol in malignant ascites promotes chemoresistance in ovarian cancer, BMC Cancer, 18 (2018) 1232.
[57] Z. Amini-Farsani, M.H. Sangtarash, M. Shamsara, H. Teimori, MiR-221/222 promote chemoresistance to cisplatin in ovarian cancer cells by targeting PTEN/PI3K/AKT signaling pathway, Cytotechnology, 70 (2018) 203-213.

[58] J. Li, Q. Li, H. Huang, Y. Li, L. Li, W. Hou, Z. You, Overexpression of miRNA-221 promotes cell proliferation by targeting the apoptotic protease activating factor-1 and indicates a poor prognosis in ovarian cancer, Int J Oncol, (2017).
[59] C. Sun, N. Li, B. Zhou, Z. Yang, D. Ding, D. Weng, L. Meng, S. Wang, J. Zhou, D. Ma, G. Chen, miR-222 is upregulated in epithelial ovarian cancer and promotes cell proliferation by downregulating P27(kip1.), Oncol Lett, 6 (2013) 507-512.
[60] R. Dai, J. Li, Y. Liu, D. Yan, S. Chen, C. Duan, X. Liu, T. He, H. Li, miR-221/222 suppression protects against endoplasmic reticulum stress-induced apoptosis via p27(Kip1)- and MEK/ERK-mediated cell cycle regulation, Biol Chem, 391 (2010) 791-801.
[61] Y. Zhang, J. Wu, J.Y. Liang, X. Huang, L. Xia, D.W. Ma, X.Y. Xu, P.P. Wu, Association of serum lipids and severity of epithelial ovarian cancer: an observational cohort study of 349 Chinese patients, J Biomed Res, 32 (2018) 336-342.
[62] A.J. Li, R.G. Elmore, I.Y. Chen, B.Y. Karlan, Serum low-density lipoprotein levels correlate with survival in advanced stage epithelial ovarian cancers, Gynecol Oncol, 116 (2010) 78-81.
[63] H. Wickham, Ggplot2 : elegrant graphics for data analysis, Use R!, Springer,, Switzerland, 2016, pp. 1 online resource.
[64] A. Kassambara, M. Kosinski, P. Biecek, survminer: Drawing Survival Curves using 'ggplot2', 2020.

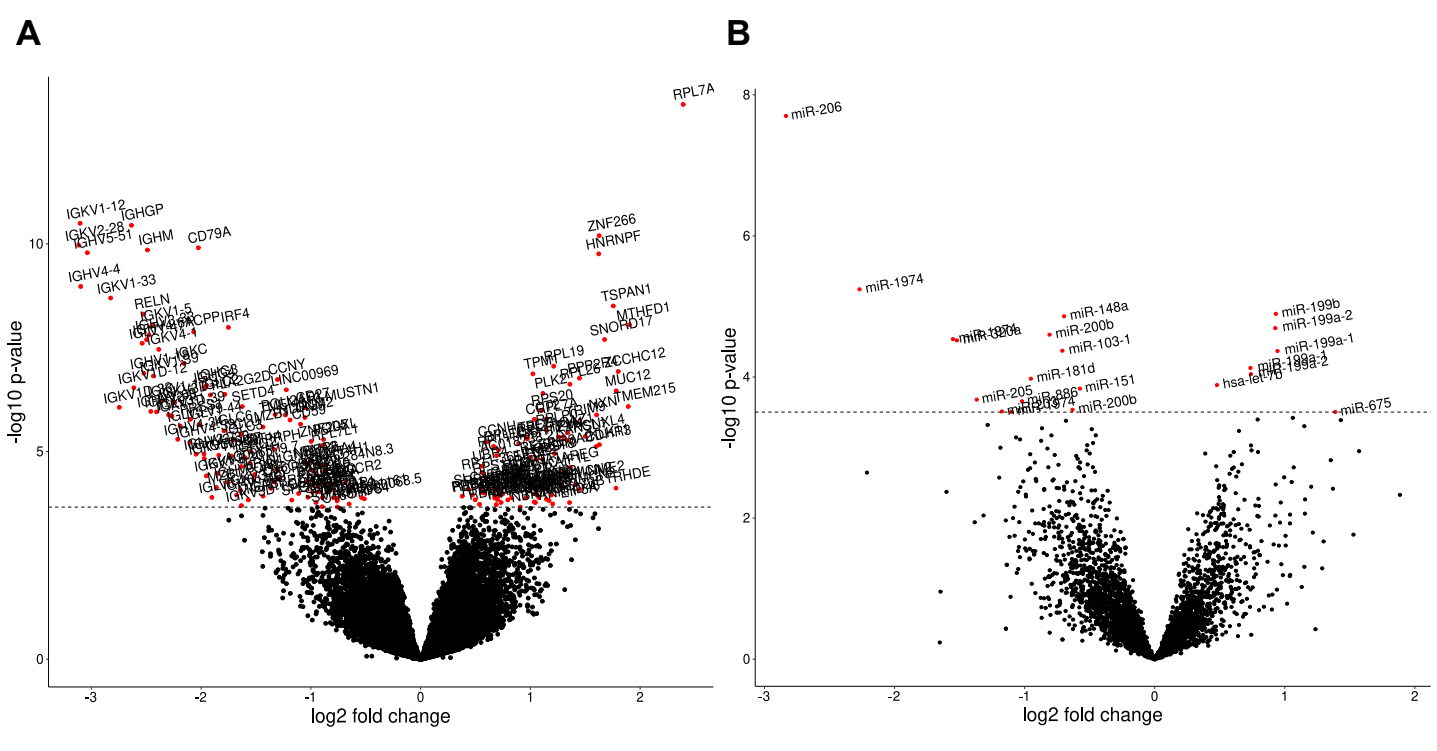
A
B
-log10 p-value
log2 fold change
RPL7A
ZNF266
HNRNPF
TSPAN1
MTHFD1
SNORD17
RPL19
CCHC12
MUC12
MEM215
IGKV1-12
IGHGP
IGKV2-28
IGHV5-51
IGHM
CD79A
IGHV4-4
IGKV1-33
RELN
IRF4
CCNY
LINC00969
SETD4
MUSTN1
miR-206
miR-1974
miR-148a
miR-200b
miR-103-1
miR-181d
miR-151
miR-205
miR-886
miR-1974
miR-200b
hsa-let-7b
miR-199b
miR-199a-2
miR-199a-1
miR-675

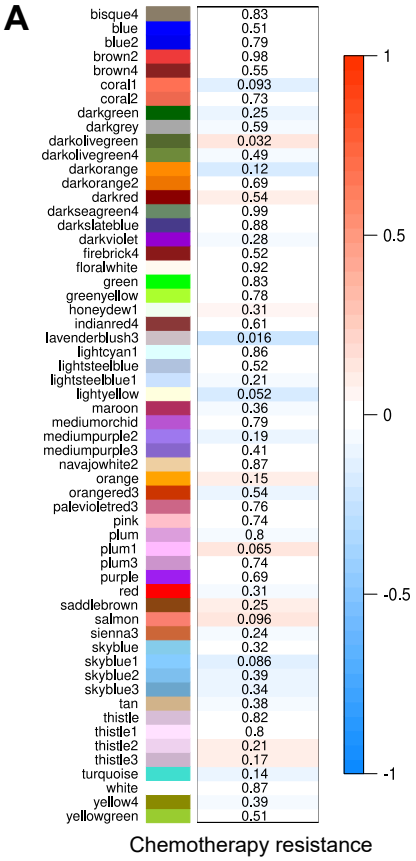
A
bisque4 0.83
blue 0.51
blue2 0.79
brown2 0.98
brown4 0.55
coral1 0.093
coral2 0.73
darkgreen 0.25
darkgrey 0.59
darkolivegreen 0.032
darkolivegreen4 0.49
darkorange 0.12
darkorange2 0.69
darkred 0.54
darkseagreen4 0.99
darkslateblue 0.88
darkviolet 0.28
firebrick4 0.52
floralwhite 0.92
green 0.83
greenyellow 0.78
honeydew1 0.31
indianred4 0.61
lavenderblush3 0.016
lightcyan1 0.86
lightsteelblue 0.52
lightsteelblue1 0.21
lightyellow 0.052
maroon 0.36
mediumorchid 0.79
mediumpurple2 0.19
mediumpurple3 0.41
navajowhite2 0.87
orange 0.15
orangered3 0.54
palevioletred3 0.76
pink 0.74
plum 0.8
plum1 0.065
plum3 0.74
purple 0.69
red 0.31
saddlebrown 0.25
salmon 0.096
sienna3 0.24
skyblue 0.32
skyblue1 0.086
skyblue2 0.39
skyblue3 0.34
tan 0.38
thistle 0.82
thistle1 0.8
thistle2 0.21
thistle3 0.17
turquoise 0.14
white 0.87
yellow4 0.39
yellowgreen 0.51
1
0.5
0
-0.5
-1
Chemotherapy resistance

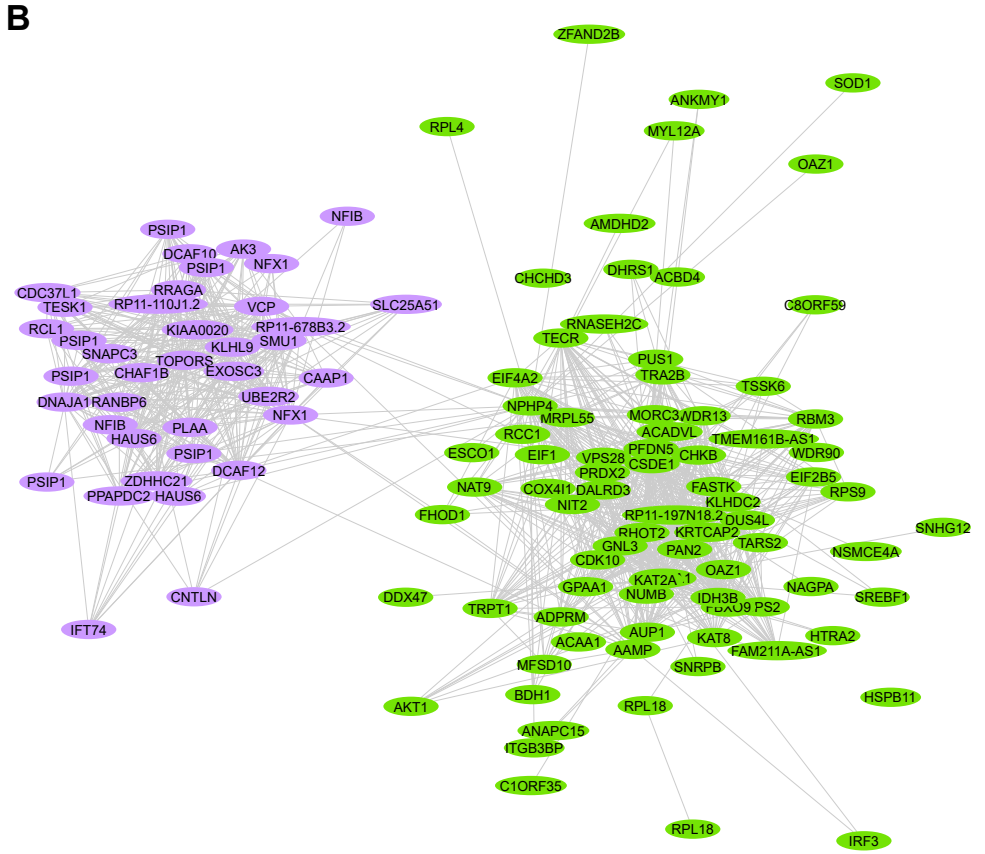
B
ZFAND2B
SOD1
ANKMY1
RPL4
MYL12A
OAZ1
NFIB
AMDHD2
PSIP1
DCAF10
AK3
PSIP1
NFX1
CHCHD3
DHRS1
ACBD4
CDC37L1
RRAGA
TESK1
RP11-110J1.2
VCP
SLC25A51
C8ORF59
RCL1
KIAA0020
RP11-678B3.2
PSIP1
SMU1
RNASEH2C
TECR
SNAPC3
KLHL9
TOPORS
PSIP1
CHAF1B
EXOSC3
CAAP1
PUS1
TRA2B
EIF4A2
TSSK6
DNAJA1
RANBP6
UBE2R2
NFX1
NPHP4
MRPL55
MORC3
WDR13
RBM3
NFIB
PLAA
HAUS6
RCC1
ACADVL
TMEM161B-AS1
PSIP1
ESCO1
EIF1
VPS28
PFDN5
CSDE1
CHKB
WDR90
PRDX2
EIF2B5
PSIP1
ZDHHC21
DCAF12
NAT9
COX4I1
DALRD3
FASTK
RPS9
PPAPDC2
HAUS6
NIT2
KLHDC2
FHOD1
RP11-197N18.2
DUS4L
SNHG12
RHOT2
KRTCAP2
GNL3
PAN2
TARS2
NSMCE4A
CDK10
OAZ1
KAT2A`.1
GPAA1
NUMB
IDH3B
NAGPA
CNTLN
DDX47
TRPT1
PBAO9
PS2
SREBF1
IFT74
ADPRM
ACAA1
AUP1
KAT8
HTRA2
AAMP
FAM211A-AS1
MFSD10
SNRPB
BDH1
HSPB11
AKT1
RPL18
ANAPC15
ITGB3BP
C1ORF35
RPL18
IRF3

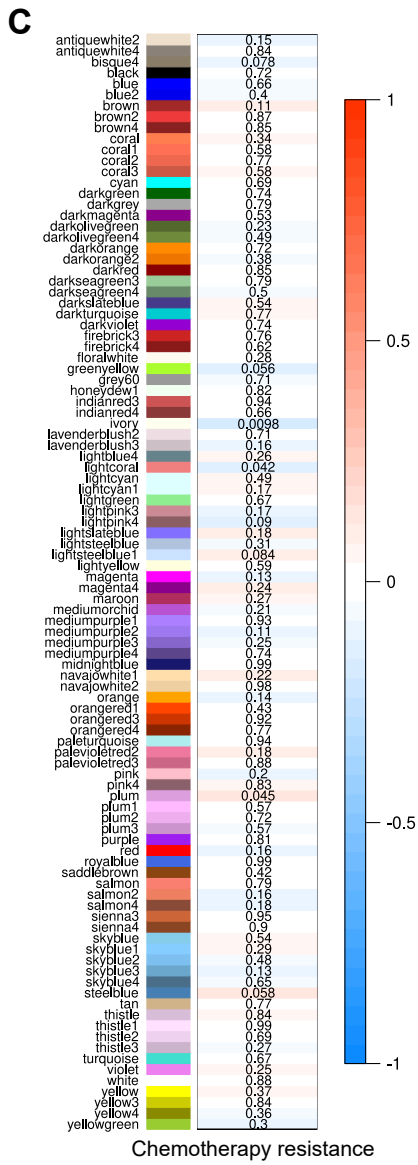
C
antiquewhite2 0.15
antiquewhite4 0.84
bisque4 0.078
black 0.72
blue 0.66
blue2 0.4
brown 0.11
brown2 0.87
brown4 0.85
coral 0.34
coral1 0.58
coral2 0.77
coral3 0.58
cyan 0.69
darkgreen 0.74
darkgrey 0.79
darkmagenta 0.53
darkolivegreen 0.23
darkolivegreen4 0.49
darkorange 0.72
darkorange2 0.38
darkred 0.85
darkseagreen3 0.79
darkseagreen4 0.5
darkslateblue 0.54
darkturquoise 0.77
darkviolet 0.74
firebrick3 0.76
firebrick4 0.62
floralwhite 0.28
greenyellow 0.056
grey60 0.71
honeydew1 0.82
indianred3 0.94
indianred4 0.66
ivory 0.0098
lavenderblush2 0.71
lavenderblush3 0.16
lightblue4 0.26
lightcoral 0.042
lightcyan 0.49
lightcyan1 0.17
lightgreen 0.67
lightpink3 0.17
lightpink4 0.09
lightslateblue 0.18
lightsteelblue 0.31
lightsteelblue1 0.094
lightyellow 0.59
magenta 0.13
magenta4 0.24
maroon 0.27
mediumorchid 0.21
mediumpurple1 0.93
mediumpurple2 0.11
mediumpurple3 0.25
mediumpurple4 0.73
midnightblue 0.99
navajowhite1 0.22
navajowhite2 0.98
orange 0.14
orangered1 0.43
orangered3 0.92
orangered4 0.77
paleturquoise 0.94
palevioletred2 0.18
palevioletred3 0.88
pink 0.2
pink4 0.83
plum 0.045
plum1 0.57
plum2 0.72
plum3 0.57
purple 0.81
red 0.16
royalblue 0.99
saddlebrown 0.42
salmon 0.79
salmon2 0.16
salmon4 0.18
sienna3 0.95
sienna4 0.9
skyblue 0.54
skyblue1 0.29
skyblue2 0.48
skyblue3 0.13
skyblue4 0.65
steelblue 0.058
tan 0.77
thistle 0.84
thistle1 0.99
thistle2 0.69
thistle3 0.27
turquoise 0.67
violet 0.25
white 0.88
yellow 0.37
yellow3 0.84
yellow4 0.36
yellowgreen 0.3
1
0.5
0
-0.5
-1
Chemotherapy resistance

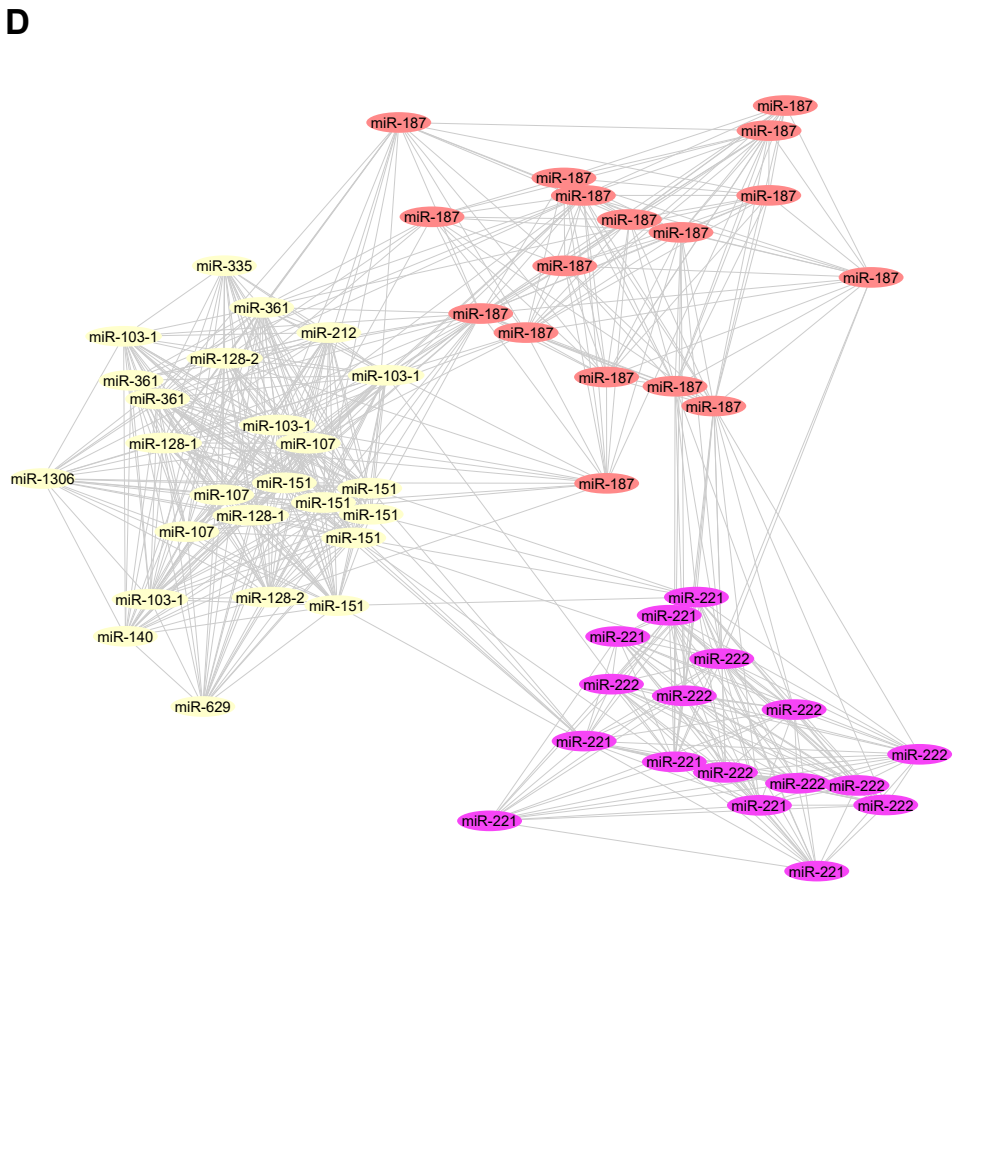
D
miR-187
miR-187
miR-187
miR-187
miR-187
miR-187
miR-187
miR-187
miR-187
miR-187
miR-187
miR-335
miR-187
miR-361
miR-187
miR-103-1
miR-212
miR-187
miR-128-2
miR-361
miR-103-1
miR-187
miR-187
miR-361
miR-187
miR-103-1
miR-128-1
miR-107
miR-1306
miR-151
miR-151
miR-187
miR-107
miR-151
miR-128-1
miR-151
miR-107
miR-151
miR-103-1
miR-128-2
miR-151
miR-221
miR-221
miR-140
miR-221
miR-222
miR-222
miR-222
miR-629
miR-222
miR-221
miR-222
miR-221
miR-222
miR-222
miR-221
miR-222
miR-221

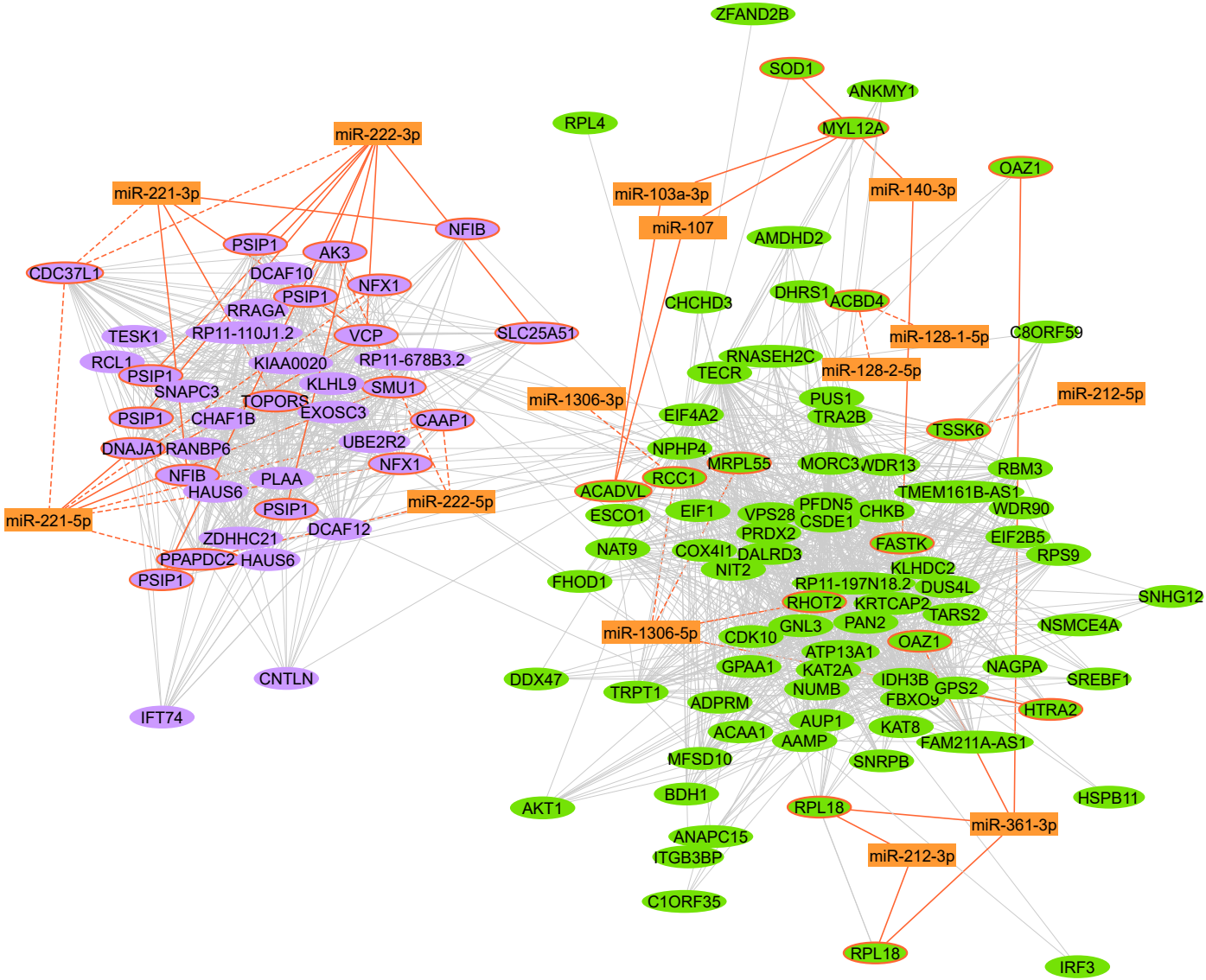
ZFAND2B
SOD1
ANKMY1
RPL4
MYL12A
miR-222-3p
OAZ1
miR-221-3p
miR-103a-3p
miR-140-3p
NFIB
miR-107
AMDHD2
PSIP1
AK3
CDC37L1
DCAF10
NFX1
PSIP1
DHRS1
ACBD4
CHCHD3
RRAGA
TESK1
RP11-110J1.2
VCP
SLC25A51
miR-128-1-5p
C8ORF59
RCL1
KIAA0020
RP11-678B3.2
RNASEH2C
PSIP1
TECR
miR-128-2-5p
SNAPC3
KLHL9
SMU1
miR-1306-3p
PUS1
miR-212-5p
TOPORS
EXOSC3
PSIP1
CHAF1B
CAAP1
EIF4A2
TRA2B
TSSK6
DNAJA1
RANBP6
UBE2R2
NPHP4
NFIB
PLAA
NFX1
MRPL55
MORC3
WDR13
RBM3
HAUS6
RCC1
ACADVL
TMEM161B-AS1
miR-221-5p
PSIP1
miR-222-5p
ESCO1
EIF1
VPS28
PFDN5
CSDE1
CHKB
WDR90
ZDHHC21
DCAF12
PRDX2
EIF2B5
NAT9
COX4I1
DALRD3
FASTK
RPS9
PPAPDC2
HAUS6
NIT2
KLHDC2
PSIP1
FHOD1
RP11-197N18.2
DUS4L
SNHG12
RHOT2
KRTCAP2
TARS2
miR-1306-5p
GNL3
PAN2
NSMCE4A
CDK10
OAZ1
ATP13A1
GPAA1
KAT2A
NAGPA
CNTLN
DDX47
IDH3B
SREBF1
TRPT1
NUMB
GPS2
FBXO9
ADPRM
HTRA2
IFT74
AUP1
KAT8
ACAA1
AAMP
FAM211A-AS1
MFSD10
SNRPB
BDH1
HSPB11
AKT1
RPL18
miR-361-3p
ANAPC15
ITGB3BP
miR-212-3p
C1ORF35
RPL18
IRF3

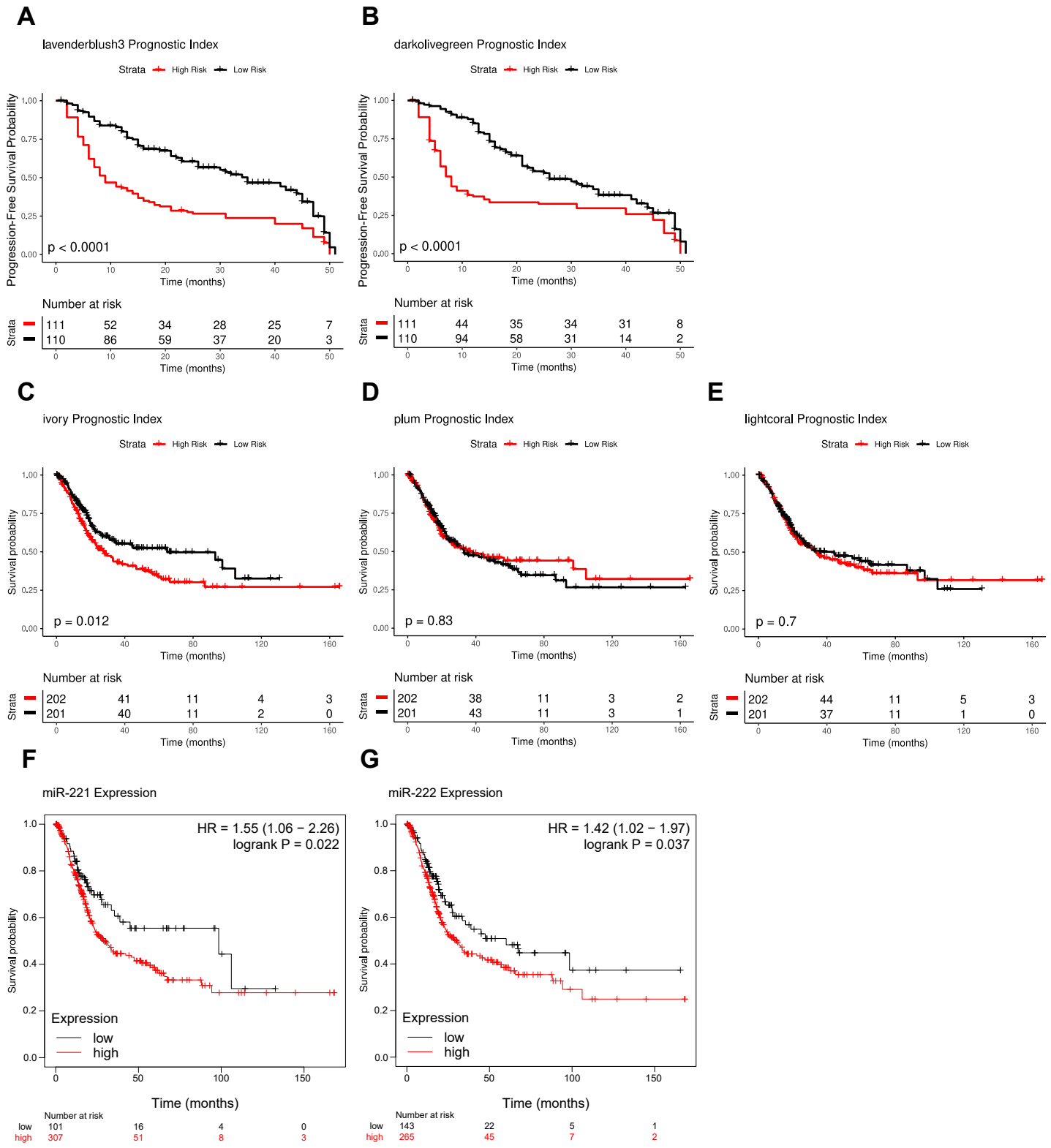
A
lavenderblush3 Prognostic Index
Strata High Risk Low Risk
Progression-Free Survival Probability
p < 0.0001
Time (months)
Number at risk
Strata
111 52 34 28 25 7
110 86 59 37 20 3
B
darkolivegreen Prognostic Index
Strata High Risk Low Risk
Progression-Free Survival Probability
p < 0.0001
Time (months)
Number at risk
Strata
111 44 35 34 31 8
110 94 58 31 14 2
C
ivory Prognostic Index
Strata High Risk Low Risk
Survival probability
p = 0.012
Time (months)
Number at risk
Strata
202 41 11 4 3
201 40 11 2 0
D
plum Prognostic Index
Strata High Risk Low Risk
Survival probability
p = 0.83
Time (months)
Number at risk
Strata
202 38 11 3 2
201 43 11 3 1
E
lightcoral Prognostic Index
Strata High Risk Low Risk
Survival probability
p = 0.7
Time (months)
Number at risk
Strata
202 44 11 5 3
201 37 11 1 0
F
miR-221 Expression
HR = 1.55 (1.06 − 2.26)
logrank P = 0.022
Survival probability
Expression
low
high
Time (months)
Number at risk
low 101 16 4 0
high 307 51 8 3
G
miR-222 Expression
HR = 1.42 (1.02 − 1.97)
logrank P = 0.037
Survival probability
Expression
low
high
Time (months)
Number at risk
low 143 22 5 1
high 265 45 7 2